

# Journal of Materials Chemistry C

Accepted Manuscript



This is an *Accepted Manuscript*, which has been through the Royal Society of Chemistry peer review process and has been accepted for publication.

*Accepted Manuscripts* are published online shortly after acceptance, before technical editing, formatting and proof reading. Using this free service, authors can make their results available to the community, in citable form, before we publish the edited article. We will replace this *Accepted Manuscript* with the edited and formatted *Advance Article* as soon as it is available.

You can find more information about *Accepted Manuscripts* in the [Information for Authors](#).

Please note that technical editing may introduce minor changes to the text and/or graphics, which may alter content. The journal's standard [Terms & Conditions](#) and the [Ethical guidelines](#) still apply. In no event shall the Royal Society of Chemistry be held responsible for any errors or omissions in this *Accepted Manuscript* or any consequences arising from the use of any information it contains.

**Properties modulation of organic semi-conductors based on a Donor-Spiro-Acceptor (D-Spiro-A) molecular design: New host materials for efficient sky-blue PhOLEDs \***

Maxime Romain,<sup>a</sup> Denis Tondelier,<sup>b</sup> Olivier Jeannin,<sup>a</sup> Bernard Geffroy,<sup>b,c\*</sup>  
Joëlle Rault-Berthelot<sup>a\*</sup> and Cyril Poriel<sup>a\*</sup>

*a. UMR CNRS 6226 "Institut des Sciences Chimiques de Rennes"  
Université de Rennes 1-Campus de Beaulieu-35042 Rennes cedex (France) Tel:(+33)2-2323-5977*

*E-mail: cyril.poriel@univ-rennes1.fr/joelle.rault-berthelot@univ-rennes1.fr*

*b. UMR CNRS 7647, LPCIM, École Polytechnique, 91128 Palaiseau, France*

*c. LICSEN/NIMBE UMR 3685, CEA Saclay, 91191 Gif Sur Yvette, France*

*E-mail: bernard.geffroy@polytechnique.edu*

*Four high triplet organic semi-conductors based on the Donor-Spiro-Acceptor design (D-Spiro-A) have been synthesized. Their physicochemical and photophysical properties have been studied, compared and discussed at the light of the nature of their respective Donor/Acceptor units. The four compounds have been used as host materials in efficient sky blue (EQE > 10 % at 10 mA/cm<sup>2</sup>) Phosphorescent Organic Light Emitting Diodes.*

In the last twenty years, many families of organic emissive materials have been developed for flat-panel displays and solid state lighting sources.<sup>1-3</sup> The design of fluorescent organic semi-conductors for green and red emission has led to highly efficient organic light emitting diodes (OLEDs).<sup>4</sup> However, the blue colour despite fantastic recent progresses in the design of fluorescent materials<sup>5-12</sup> and in the device architectures<sup>13</sup> remains less efficient and less stable than the other colours.<sup>4</sup> In addition, in the last fifteen years, it has been demonstrated that highly efficient blue emission should not be obtained in OLED devices using pure organic singlet exciton emissive layers (EML) but should require more sophisticated EML in which a blue phosphor is doped in an organic host material to harvest both singlet and triplet excitons. Such devices, the phosphorescent Organic Light-Emitting Diodes (PhOLEDs) have then attracted fantastic interest.<sup>14-18</sup> One of the weakest links of this technology remains the design of highly efficient host materials for blue phosphors. Indeed, the prerequisites for an ideal host for a blue dopant are (i) a high triplet energy ( $E_T$ ) to avoid reverse energy transfers from the guest back to the host, (ii) a high glass-transition temperature ( $T_g$ ) and decomposition temperature ( $T_d$ ) for stability, (iii) matching HOMO-LUMO levels for injection of the charges (iv) good and balanced charge transporting properties to insure efficient recombination in the dopant. For industrial production, long and sophisticated chemical syntheses of the host should be also clearly proscribed. Bipolar molecules incorporating hole

\* Electronic Supplementary Information (ESI) available: Materials and methods, experimental details; synthesis and characterization of all compounds, absorption spectra in various solvents, DSC, copy of NMR spectra, Green devices performance.

and electron transporting units to adjust the energy levels of frontier orbitals appear to date the most promising candidates for PhOLED applications.<sup>2, 16-22</sup> Thus, when designing bipolar hosts, one should carefully consider the selection of the donor/acceptor pair and their relative positions within the dye. Indeed, the donor/acceptor combination often results in  $\pi$ -conjugation enlargement, which would accordingly reduce the singlet and triplet energies. Therefore, to obtain bipolar hosts with high  $E_T$ , the  $\pi$ -conjugation and the electronic coupling between the donor and the acceptor units must be restricted. The choice of the linker and the relative position of the donor and acceptor units must then be carefully performed.

To date, many successful design strategies have been developed to gather all the above mentioned properties in a single host and particularly to disrupt the  $\pi$ -conjugation. Some relevant examples are presented in Chart 1.

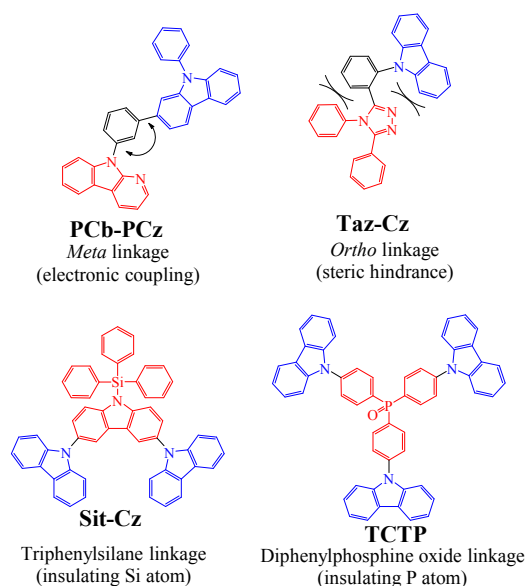


Chart 1. Different design strategies for  $\pi$ -conjugation disruption

First, it is known that electronic coupling through a *meta* linkage is inherently weaker than through a *para* one<sup>5, 23-27</sup> and this strategy has often been used to connect a hole transporting and an electron transporting unit in a host material.<sup>21, 24, 28, 29</sup> Thus, the *meta* linkages efficiently disrupt the  $\pi$ -conjugation between a donor and an acceptor as for instance in 9-(3-(diphenylcarbazol-3-yl)phenyl)- $\alpha$ -carboline (**PCb-PCz**, Chart 1), in which the N-phenylcarbazole donor unit is separated from the pyridindole acceptor unit by a *meta*-substituted phenyl unit (HOMO: -5.75 eV, LUMO: -2.31 eV,  $E_T = 2.74$  eV).<sup>21</sup> A second approach widely developed in the literature consists to introduce a steric congestion within the dye to hinder the planarization between two connected  $\pi$ -systems.<sup>30-33</sup> This 'steric hindrance' strategy is most of the time performed through the incorporation of a sterically hindered *ortho* linkage efficiently leading to a  $\pi$ -conjugation restriction. For example, in **Taz-Cz** (Chart 1), the carbazole and 1,2,4-triazole are both oriented with a dihedral angle larger than  $45^\circ$  with the central benzene ring, efficiently disrupting the  $\pi$ -conjugation between the carbazole and the triazole (HOMO: -5.7 eV, LUMO: -2.3 eV,  $E_T$  of 3.09 eV).<sup>31</sup>

Using an insulating heteroatom is also an efficient strategy to obtain high  $E_T$  materials with short  $\pi$ -conjugated pathway. Thus, silicium (silane),<sup>2, 18, 34, 35</sup> and phosphoryl group (P=O),<sup>2, 18, 20, 29, 36, 37</sup> may act as an effective breaking point of the  $\pi$ -conjugation between the main core of the molecule and the outer groups linked to the heteroatom (phenyl for example in the case of the efficient electron transporting diphenylphosphine oxide unit). Thus, the electronic structure of the bipolar molecules is almost identical to those of the corresponding central core, which is a crucial point to avoid the decrease of  $E_T$ .<sup>20</sup> For example, in the 9'-triphenylsilylanyl-9'H-[9,3',6',9'']ter-carbazole (**Sit-Cz**), the direct connexion of the silane to a carbazole unit through the nitrogen atom renders this carbazole electro-deficient (HOMO: -5.54 eV, LUMO :-2.3 eV,  $E_T$ : 3.0 eV).<sup>38</sup> Similarly, in the star-shaped molecule 4,4',4''-tri(N-carbazolyl)triphenylphosphine oxide (**TCTP**), the electron-acceptor phosphine oxide unit is used both as the core and as the electron donor, the carbazole moiety, acting as the branch.<sup>39</sup> HOMO/LUMO levels respectively lie at -5.25 eV/-1.67 eV, and the disrupted conjugation via phosphine-oxide linkage preserves a high  $E_T$  of 3.03 eV.

More recently, another promising and simple molecular design based on a  $\pi$ -conjugation breaking induced by an insulating spiro bridge (called *D-Spiro-A* design) has been introduced in literature. This design which allows to separate the HOMO and LUMO levels has a great potential in Thermally Activated Delayed Fluorescence (TADF)<sup>40, 41</sup> but remains rarely used to date in the field of host materials for blue phosphorescent dopants.<sup>35, 42-44</sup> Our attention for this design was to avoid the introduction of pendant hole or electron transporting units, strongly simplifying the molecular structure and hence the chemical synthesis. In the present work, we wish to report a structure-properties relationship study of new donor/acceptor molecules based on this *D-Spiro-A* design. These semi-conductors present different electronic properties and have been used as host in sky blue PhOLEDs leading in some case to high efficiencies (EQE>10% at 10 mA.cm<sup>-2</sup>) The large differences observed in term of PhOLED efficiencies highlight the importance of the donor/acceptor combination used in the molecular design of the host. Such structure-properties relationship study may provide interesting insights for the development of future materials for optoelectronics. Thus, in this work, as a development to our preliminary note on the dye **SPA-TXO<sub>2</sub>** (Scheme 1),<sup>45</sup> we have investigated through a *D-Spiro-A* design, two hole transporting moieties, namely N-phenylacridine (PA)<sup>43</sup> and thioxanthene (TX) and two electron transporting moieties, namely thioxanthene dioxide (TXO<sub>2</sub>) and diazafluorene (DAF) (Scheme 1). These four molecular fragments are briefly described below.

In PA, two phenyl rings of a triphenylamine unit are connected by a methylene unit forming a hexagon. Structurally, the presence of this hexagon renders the N-phenyl acridine unit more similar to a triphenylamine than to a N-phenylcarbazole unit.<sup>46</sup> The strong electron rich nature of PA unit has been previously exploited in TADF,<sup>40, 41, 47</sup> in non-doped blue OLEDs,<sup>48</sup> and in host materials for blue PhOLEDs.<sup>35, 42, 43, 49, 50</sup>

TX is the structural analogue of xanthene, possessing an intracyclic sulphur atom instead of an oxygen atom. Recently, Yam et al have reported various spiro-configured dyes based on the connection of a TX (and TXO<sub>2</sub>) unit with a 2,7-bis(diphenylamine)fluorene leading to

very promising donor materials in the construction of high performance organic photovoltaic devices.<sup>51</sup>

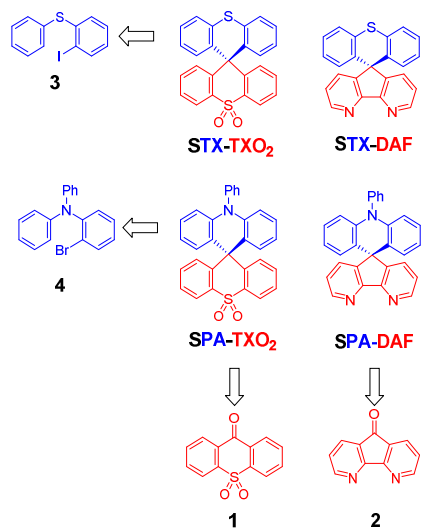
TXO<sub>2</sub> is the oxidized analogue of TX. The presence of the sulfone in TXO<sub>2</sub> leads to better electron injection and transport abilities due to the depress of the LUMO level.<sup>12</sup> Indeed, sulfones have been efficiently incorporated (i) in highly efficient blue emitting materials,<sup>52-54</sup> (ii) in host materials for PhOLEDs,<sup>55-57</sup> and (iii) in electron-transporting materials.<sup>58</sup> However, the use of TXO<sub>2</sub> fragment remains scarce and our group, in a preliminary note, has recently demonstrated its potential in the design of host for blue PhOLEDs.<sup>45</sup> Thus, by a simple oxidation step, it is hence possible to switch from hole transporting properties in TX to electron transporting properties in TXO<sub>2</sub>, highlighting the versatility of these systems.

Electron acceptor DAF may be regarded as a bipyridine unit possessing then a similar molecular arrangement than that of the well-known bridged biphenyl, namely fluorene. The strong electron affinity of this unit<sup>59, 60</sup> could decrease the LUMO energy level, thereby improving the electron injection and transport properties of the materials. Up to now, DAF fragments have been investigated in many research fields, such as electron-transporting materials,<sup>61</sup> organic emitters,<sup>59, 62</sup> and sensors.<sup>63</sup> DAF fragment is also an interesting platform to coordinate various metals such as cadmium,<sup>64</sup> zinc,<sup>64</sup> rhenium,<sup>65</sup> silver<sup>66</sup> and iridium.<sup>67, 68</sup> However, to the best of our knowledge, DAF unit remains rarely incorporated in host materials for PhOLED.<sup>60, 61, 69</sup>

## Results and discussion

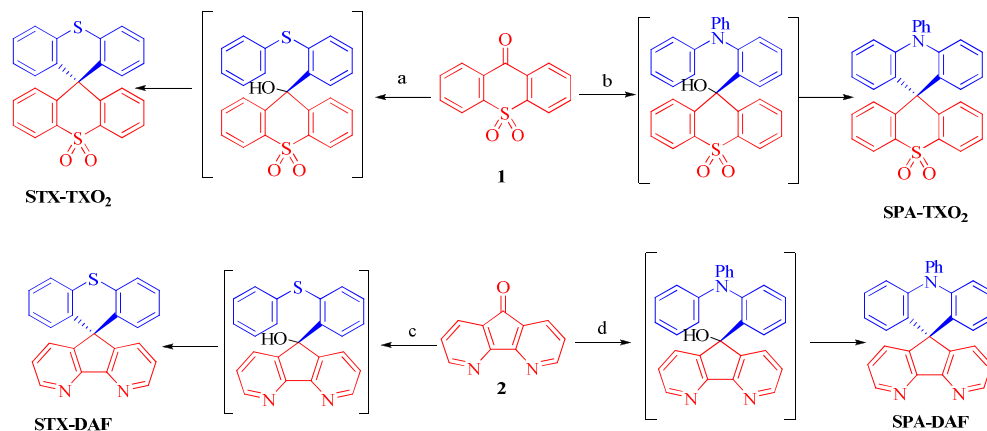
### Synthesis

It is crucial for the future of organic optoelectronics to establish short and very efficient synthetic approaches of organic materials. Herein, all the dyes have been synthesised through a one pot very efficient route using common and easily synthesizable intermediates. Thus, the two halogeno-aryls **3** and **4**, judiciously coupled with the two ketones **1** and **2** provide **STX-TXO<sub>2</sub>** (**3** + **1**), **STX-DAF** (**3**+**2**), **SPA-TXO<sub>2</sub>** (**4**+**1**) and **SPA-DAF** (**4**+**2**) (Scheme 1).



Scheme 1. Retrosynthetic analysis of the four dyes investigated in this work: **STX-TXO<sub>2</sub>**, **STX-DAF**, **SPA-TXO<sub>2</sub>** and **SPA-DAF**

Regarding the TXO<sub>2</sub> derivative (Scheme 2, top), a lithium-bromine exchange was first performed on either 2-bromo-N,N-diphenylaniline **4** or (2-iodophenyl)(phenyl)sulfane **3** followed by the trapping of the lithiated intermediate by ketone 9*H*-thioxanthen-9-one-10,10-dioxide **1** (obtained by oxidation of commercially available 9*H*-thioxanthen-9-one with hydrogen peroxide, see SI). Electrophilic intramolecular cyclization reaction of the resulting dioxothioxanthenols (not isolated) in acidic media (HCl in acetic acid), afforded SPA-TXO<sub>2</sub> or STX-TXO<sub>2</sub> in high yield (78 and 88 % respectively over the three steps). This one pot synthetic strategy is very simple, easy to perform, highly efficient for a gram scale synthesis and is versatile to many different donor and acceptors fragments.



Scheme 2 : Synthesis of STX-TXO<sub>2</sub>, SPA-TXO<sub>2</sub>, STX-DAF and SPA-DAF

**a**) (2-iodophenyl)(phenyl)sulfane **3**, nBuLi, THF from -80 °C to 20 °C then HCl, AcOH reflux 88%, **b**) 2-bromo-N,N-diphenylaniline **4**, nBuLi, THF from -80 °C to 20 °C then HCl, AcOH reflux 78%. **c**) (2-iodophenyl)(phenyl)sulfane **3**, nBuLi, THF from -80 °C to 20 °C then MsOH, 1,2-dichlorobenzene reflux 39%, **d**) 2-bromo-N,N-diphenylaniline, nBuLi, THF from -80 °C to 20 °C then MsOH, 1,2-dichlorobenzene, reflux 47% .

An identical strategy has been developed to synthesise STX-DAF and SPA-DAF (Scheme 2, bottom) involving first the synthesis of the known diazafluorenone **2** (obtained by oxidation and ring contraction of phenanthroline in water in presence of KMnO<sub>4</sub> and KOH, see SI).<sup>70</sup> Reaction of **2** with the corresponding lithiated intermediates derived from **3** or **4** was then performed leading to the corresponding diazafluorenol derivatives. However the intramolecular cyclization reaction in similar conditions than those exposed above (HCl/CH<sub>3</sub>CO<sub>2</sub>H, Scheme 2) did not occur, highlighting the very different reactivity of diazafluorenols vs dioxothioxanthenols. X-ray structure of the triphenylamine diazafluorenol shows short distances (*ca* 2 Å, see Figure in SI) between hydrogen atom of the hydroxide unit of one molecule and a nitrogen atom of the diazafluorene unit of a second molecule. These short distances sign the presence of intermolecular interactions that may explain a stabilization of the diazafluorenol and hence its weak reactivity. In addition, the nitrogen atoms of the diazafluorene unit might be protonated during the cyclisation step decreasing again its reactivity. Using more drastic conditions and 3 equivalents of methane sulfonic acid at high temperature (180 °C in 1,2-dichlorobenzene), target compounds STX-DAF (yield : 39%) and SPA-DAF (yield : 47 %) were finally isolated. It should be noted that in the course of this work, the synthesis of SPA-DAF as an intermediate building block has been reported by

Adachi and coworkers using Eaton's reagent to cyclise the diazafluorene derivative.<sup>40</sup> However, the properties of **SPA-DAF** were not reported in this work.

### <sup>1</sup>H NMR studies

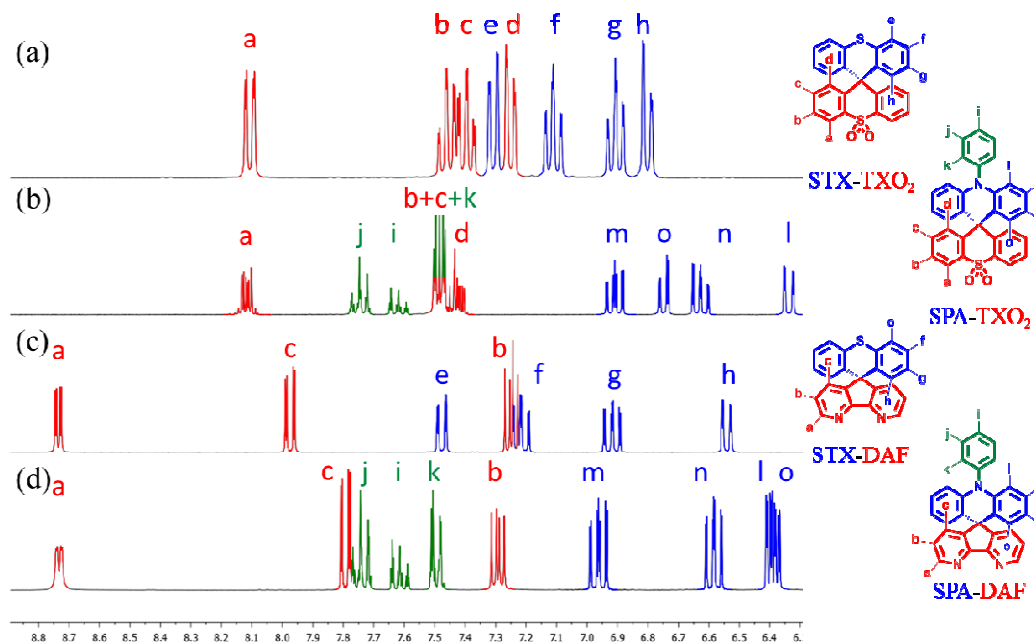


Figure 1. Portion <sup>1</sup>H of NMR Spectra of (a) **STX-TXO<sub>2</sub>**, (b) **SPA-TXO<sub>2</sub>**, (c) **STX-DAF** and (d) **SPA-DAF** in CD<sub>2</sub>Cl<sub>2</sub>.

<sup>1</sup>H NMR spectroscopy is an interesting tool to evaluate the strength of electron withdrawing/donating moieties on the environment. Thus, the effect of the incorporation of heteroatoms in the spirobifluorene like molecules described herein can be interestingly visualized through NMR spectroscopy. The complete assignments of all signals have been performed by 2D NMR spectroscopy experiments (HMBC, HMQC, <sup>1</sup>H/<sup>1</sup>H COSY, see SI).

For **STX-TXO<sub>2</sub>** and **SPA-TXO<sub>2</sub>**, one can note that the hydrogen atoms (Ha-d) of the **TXO<sub>2</sub>** fragment (Figures 1a and 1b, red lines) are centred around 7.35 ppm except Ha, which appear to be deshielded due to the proximity of the sulfone unit. Considering the chemical shift of benzene (7.35 ppm in CD<sub>2</sub>Cl<sub>2</sub>)<sup>71</sup> one can conclude that the **TXO<sub>2</sub>** is a weak electron withdrawing unit. On the opposite, the signals Hf-h of the TX unit and Hl-o of the PA core appear to be shielded highlighting their electron-donating nature. We can note that the incorporation of the nitrogen atom within the PA unit, leads to a stronger shielding than that observed for the sulphur in TX, highlighting the stronger electron-donating nature of the former. This will be confirmed by electrochemistry (see below). It should be mentioned that the resonances of the pendant phenyl ring of the PA (Hi-k) are found at low field ( $\delta$  7.58/7.8 ppm) meaning that the free doublet of the nitrogen atom is conjugated with the acridine and not with the phenyl unit.

Similar effects have been detected for **STX-DAF** and **SPA-DAF** with in addition two very low field resonances recorded at 8 and 8.65 ppm (respectively assigned to Hc in  $\gamma$  position

and to Ha in  $\beta$  position of the nitrogen atom of the DAF). This highlights the strong electron-withdrawing nature of DAF fragment.

### Structural properties

The four compounds have been crystallized by vapour diffusion of pentane in  $\text{CDCl}_3$  solution in order to confirm their molecular structures by X-ray crystallography and to study the structural characteristics (See X-Ray in SI). **STX-TXO<sub>2</sub>** and **SPA-TXO<sub>2</sub>** both crystallized in a triclinic system. **STX-TXO<sub>2</sub>** asymmetric unit contains two different molecules and one molecule of  $\text{CDCl}_3$  whereas that of **SPA-TXO<sub>2</sub>** contains only one molecule without solvent. **STX-DAF** crystallizes in an orthorhombic system with only one molecule per unit and **SPA-DAF** crystallizes with two molecules of solvents in a monoclinic system.

The molecular radius of each molecule (distance from the spiro carbon atom to the farthest carbon atom, green arrow in figure 2) has been evaluated at 7.14/7.10 Å for **SPA-TXO<sub>2</sub>** and **SPA-DAF** *resp.* and at 4.36/4.34 Å for **STX-TXO<sub>2</sub>** and **STX-DAF** *resp.* For the four molecules, this radius is imposed by the donor groups (**TX** or **DAF**) which are the longest units.

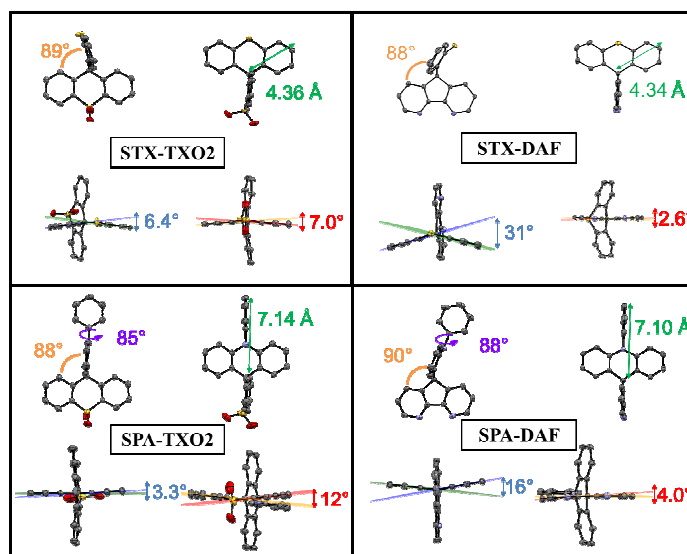


Figure 2. Molecular structure from X-Ray crystallography of **STX-TXO<sub>2</sub>** (top left), **STX-DAF** (top right), **SPA-TXO<sub>2</sub>** (bottom left), and **SPA-DAF** (bottom right) (ellipsoid probability at 50% level), hydrogen atoms have been omitted for clarity.

In all molecules, the donor and the acceptor fragments are almost orthogonal with a twist angle (value in orange in figure 2) varying from 88° for both **STX-DAF** and **SPA-TXO<sub>2</sub>**, 89° for **STX-TXO<sub>2</sub>** to 90° for **STX-DAF**. This orthogonality between the donor and the acceptor moiety is at the origin of the absence of significant  $\pi$ -conjugation between them. Additionally, in the PA derivatives, the angle between the mean plane of the acridine units (indicated in purple in figure 2) and that of the attached phenyl is of 85/88° in **SPA-TXO<sub>2</sub>** and **SPA-DAF** *resp.* This large angle indicates a second  $\pi$ -conjugation breaking at the nitrogen atom between the acridine unit and the phenyl. As discussed below, these  $\pi$ -conjugation breakings are essential to keep the high  $E_T$  (see below).



For each aromatic unit, a torsional angle has been defined as the dihedral angle between the two external benzene rings of each unit (values in blue for the donor units and in red for the acceptor units in figure 2).

For the donor units, the TX torsion angles are impressively different depending of the acceptor core. Thus, a small angle of  $6.4^\circ$  is recorded for **STX-TXO<sub>2</sub>** and a very large angle of  $31^\circ$  is recorded for **STX-DAF**. Similarly, the torsion angles measured in the PA units are 5 times larger for **SPA-DAF** ( $16^\circ$ ) than for **SPA-TXO<sub>2</sub>** ( $3.3^\circ$ ). Thus, the donor fragments in **SPA-DAF** and **STX-DAF** are strongly more distorted than in their counterparts **SPA-TXO<sub>2</sub>** and **STX-TXO<sub>2</sub>**. The presence of the DAF unit within the dyes leads hence to a very distorted donor with large dihedral angles. This feature may be assigned to the packing forces induced by the presence of the DAF. In addition and regardless of the acceptor, the PA units are always less distorted than the TX units surely due to the presence in PA of a pendant phenyl ring which provides a certain degree of rigidity.

For the acceptor units, the **TXO<sub>2</sub>** torsion angle is of  $7^\circ$  for **STX-TXO<sub>2</sub>** and of  $12^\circ$  for **SPA-TXO<sub>2</sub>** whereas this torsion angle is very weak in the case of the **DAF** unit:  $2.6^\circ$  for **STX-DAF**, and  $4.0^\circ$  for **SPA-DAF**. Thus, the very rigid **DAF** unit only allows very weak deformations due the presence of the C-C bond in  $\alpha$  position of the nitrogen atoms. Such conformational locking is very similar to that observed for fluorene unit. Oppositely, the presence of the sulphur atom linking the two phenyl groups in the **TXO<sub>2</sub>** unit allows some deviations from planarity.

### Thermal Properties

Before any possible OLED applications and in order to confirm the interest of the present *D-spiro-A* design, the four compounds have been studied by thermogravimetric analysis (TGA) (Figure 3) and differential scanning calorimetry (DSC) (see SI).

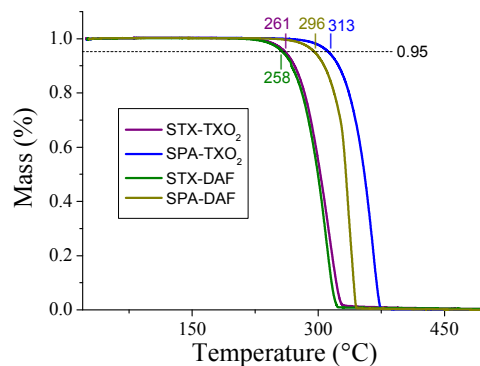


Figure 3. TGA curves of **STX-TXO<sub>2</sub>** (violet line), **STX-DAF** (green line), **SPA-TXO<sub>2</sub>** (blue line) and **SPA-DAF** (yellow green line)

The decomposition temperature  $T_d$ , is defined as the temperature corresponding to 5% of mass loss.<sup>72</sup> Herein, these temperatures are recorded at 261/258 °C for **STX-TXO<sub>2</sub>** / **STX-DAF** and at 313/296 °C for **SPA-TXO<sub>2</sub>** / **SPA-DAF** respectively (Figure 3). As a complete mass loss then occurs, we believe that this mass loss is attributed to a sublimation process as

previously observed for other  $\pi$ -conjugated systems.<sup>24</sup> Thus, the presence of the PA unit within the dye leads to a material with a higher  $T_d$  (by ca 40/50°) than that obtained with the TX unit. DSC studies reveal no phase transition between the room temperature and the decomposition of the molecules (see SI). The rigid molecular structure of the two spiroannulated fragments is at the origin of the interesting thermal properties of the four molecules.

### Electrochemical Properties

Electrochemical properties have been investigated by cyclic voltammetries (CV) in  $\text{CH}_2\text{Cl}_2$  in oxidation and reduction (Figure 4 and Table 1, potentials given vs SCE). In oxidation, the two TX derivatives present an irreversible oxidation with maximum at 1.55 V for **STX-TXO<sub>2</sub>** (violet line) and at 1.48 V for **STX-DAF** (green line). From their respective onset oxidation potentials (1.42/1.34 V), their HOMO energy levels were determined at -5.79/-5.74 eV for **STX-TXO<sub>2</sub>** / **STX-DAF**.

In the PA series, the two derivatives are oxidized at even lower anodic potentials and present one reversible oxidation wave with maximum at 1.14 V for **SPA-TXO<sub>2</sub>** and two very close oxidation waves with maxima at 1.11/1.20 V for **SPA-DAF**. For **SPA-DAF**, recording the CV up to the first oxidation wave only shows an irreversible oxidation wave indicating a high reactivity of the **SPA-DAF<sup>+</sup>** species at the timescale of the CV (see Figure in SI). However, when reaching the second oxidation wave, an adsorption-like reduction peak is observed showing that the species formed during the two oxidation processes are strongly adsorbed at the electrode surface. From their onset potentials measured at 1.03/0.95 V for **SPA-TXO<sub>2</sub>** / **SPA-DAF** *resp.*, the HOMO levels were calculated at -5.42 eV for **SPA-TXO<sub>2</sub>** and -5.35 eV for **SPA-DAF**.

In the light of electronic distribution of the HOMO (DFT calculations performed at the Gaussian 09 B3LYP/6-311+G(d,p) level of theory, Figure 6), the first oxidations are assigned to the oxidation of the electron rich fragment, namely TX unit in **STX-TXO<sub>2</sub>** / **STX-DAF** and to the PA core in **SPA-TXO<sub>2</sub>** / **SPA-DAF**.

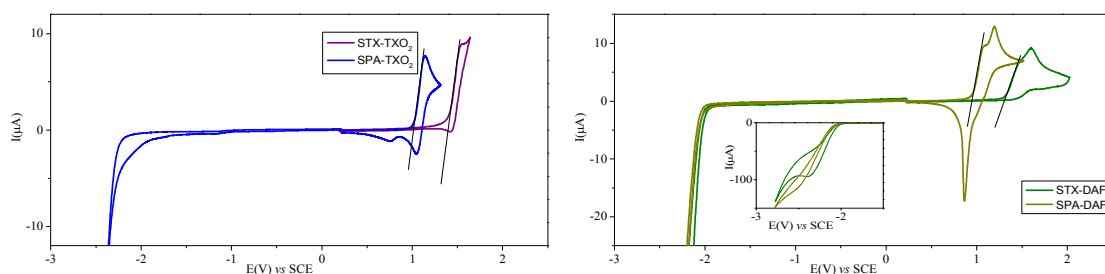


Figure 4. Cyclic voltammetry (100 mV/s) in  $\text{CH}_2\text{Cl}_2$ /[Bu<sub>4</sub>N][PF<sub>6</sub>] 0.2 M of **STX-TXO<sub>2</sub>** (violet line) and **SPA-TXO<sub>2</sub>** (blue line) (left) and of **STX-DAF** (green line), and **SPA-DAF** (yellow green line) (right).

In reduction (Figure 4), the TXO<sub>2</sub> derivatives are reduced at potential values closed to that of the electrolytic medium reduction and their onset potentials are detected at ca -2.4 V, the LUMO levels lying hence around -2.0 eV. The DAF derivatives are reduced at less negative potentials than those of TXO<sub>2</sub> derivatives and an irreversible reduction wave is observed (see

inset in figure 4, right) with a maximum recorded at -2.42/-2.5 V for **STX-DAF** / **SPA-DAF** *resp.* Thus, the LUMO levels of **STX-DAF** and **SPA-DAF** have been evaluated at -2.34 / -2.31 eV, being ca 0.3 eV lower than the LUMO levels of the TXO<sub>2</sub> derivatives (-2.0 eV). This feature clearly indicates the stronger electron accepting capability of DAF compare to that of TXO<sub>2</sub> and its potential to depress the LUMO level. Thus, **SPA-DAF** possessing the strongest donor/acceptor combination, displays an electrochemical gap  $\Delta E_{\text{elec}}$  of 3.04 eV being strongly more contracted than that of **STX-TXO<sub>2</sub>** (3.79 eV), which possesses the weakest donor/acceptor combination (Figure 5). **STX-DAF** and **SPA-TXO<sub>2</sub>** possess therefore intermediate values of 3.36 and 3.43 eV respectively. For comparison purpose, structurally related 9,9'-spirobifluorene (**SBF**)<sup>72, 73</sup> possessing two spiro-connected fluorene units possesses a wide  $\Delta E_{\text{elec}}$  of 4.05 eV (HOMO: -5.94 eV, LUMO: -1.89 eV),<sup>33</sup> widened by more than 1 eV compared to that of **SPA-DAF**. Thus, compared to **SBF**, we can note that the TX unit leads to dyes with higher HOMO level (-5.94 eV for **SBF** vs -5.70/-5.79 eV for **STX-DAF**/**STX-TXO<sub>2</sub>**) and that the TXO<sub>2</sub> unit leads to dyes with slightly lower LUMO level (-1.89 eV for **SBF** vs -2.0 eV for both **STX-TXO<sub>2</sub>** and **SPA-TXO<sub>2</sub>**). The effect of these fragments on the molecular orbitals energy levels are hence relatively weak compared to those of fluorene. Oppositely, the PA/DAF units lead to a strong increase/decrease of the HOMO/LUMO energy levels compared to **SBF**. Thus, the PA/DAF combination seems to be the more attractive leading to the smallest gap, 3.04 eV, in the series whereas the TX/TXO<sub>2</sub> combination leads to the widest gap in the series, 3.79 eV, highlighting not only the efficiency of the present design to tune the electronic properties of spiro-connected compounds but also the importance of the chosen Donor/Acceptor combination.

Compared to previously reported structurally related PA compounds bridged by a spiroanthracenone (HOMO/LUMO: -5.50/-1.90 eV) or by two phenyls units (HOMO/LUMO: -5.42/-1.74 eV),<sup>42</sup> **SPA-TXO<sub>2</sub>** and **SPA-DAF** (HOMO: -5.42 and -5.35 eV respectively) have (i) a very similar HOMO energy level, due to the presence of the PA unit, but (ii) a lower LUMO energy level (LUMO: -2 eV and -2.31 eV) due to the presence of either the TXO<sub>2</sub> or the DAF unit instead of the anthracenone core. Thus, the present design allows selectively tuning the LUMO energy level without changing that of the HOMO.

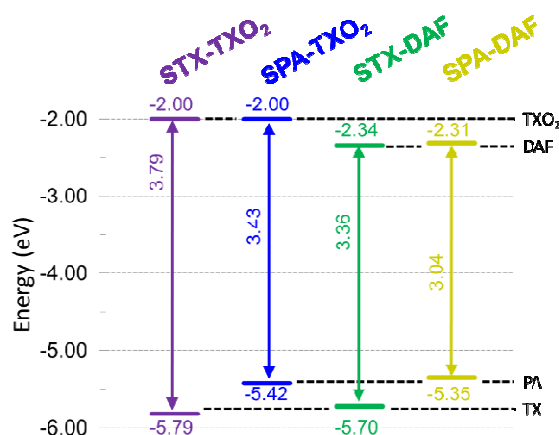


Figure 5. HOMO/LUMO energy levels and  $\Delta E_{\text{el}}$  (eV) obtained from electrochemical investigations

**Table 1.** Selected theoretical calculations, electrochemical and thermal data of the four dyes

	Electrochemical properties <sup>a</sup>					Theoretical calculations		Thermal properties
	E <sup>ox</sup> (V)	E <sub>onset<sup>ox</sup></sub> (V) / HOMO (eV)	E <sup>red</sup> (V)	E <sub>onset<sup>red</sup></sub> (V) / LUMO (eV)	ΔE <sub>el</sub> (eV)	HOMO/LUMO	ΔE <sub>theo</sub> (eV)	Td (°C)
<b>STX-TXO<sub>2</sub></b>	1.55	1.39 / -5.79	–	-2.40 / -2.00	3.79	-6.03/-1.59	4.44	261
<b>SPA-TXO<sub>2</sub></b>	1.14	1.02 / -5.42	–	-2.40 / -2.00	3.43	-5.57/-1.44	4.13	313
<b>STX-DAF</b>	1.48/1.60	1.30 / -5.70	-2.41	-2.06 / -2.34	3.36	-5.87/-1.87	4.00	258
<b>SPA-DAF</b>	1.11/1.20	0.95 / -5.35	~ -2.5	-2.09 / -2.31	3.04	-5.49/-1.72	3.77	296

a/ all potentials are given vs SCE

### *Theoretical calculations*

Geometry optimization of the four dyes in the singlet and triplet states was performed using Density Functional Theory (DFT) at the Gaussian 09 B3LYP/6-311+G(d,p) level of theory. All the results are reported in Table 1 and in Figure 6. The electronic distribution and the energy levels of HOMOs and LUMOs (and the corresponding energy gaps ΔE<sub>theo</sub>) have been determined on optimized geometries. The same tendency is observed between the HOMO/LUMO values determined by CVs and those obtained by theoretical calculations. The HOMO levels (calculated at -5.49 and -5.57 eV) of **SPA-DAF** and **SPA-TXO<sub>2</sub>** are exclusively centred on the PA units (Figure 6) in accordance with an electron transfer centred on this unit as suggested above in the electrochemical part. One can note that there is no electron density on the pendant N-phenyl meaning that the electronic properties of PA unit are independent of this pendant phenyl. HOMO of **STX-TXO<sub>2</sub>** and **STX-DAF** are mainly localized on the TX unit, leading to deeper HOMO energy levels (-6.03 and -5.87 eV) than those of PA derivatives.

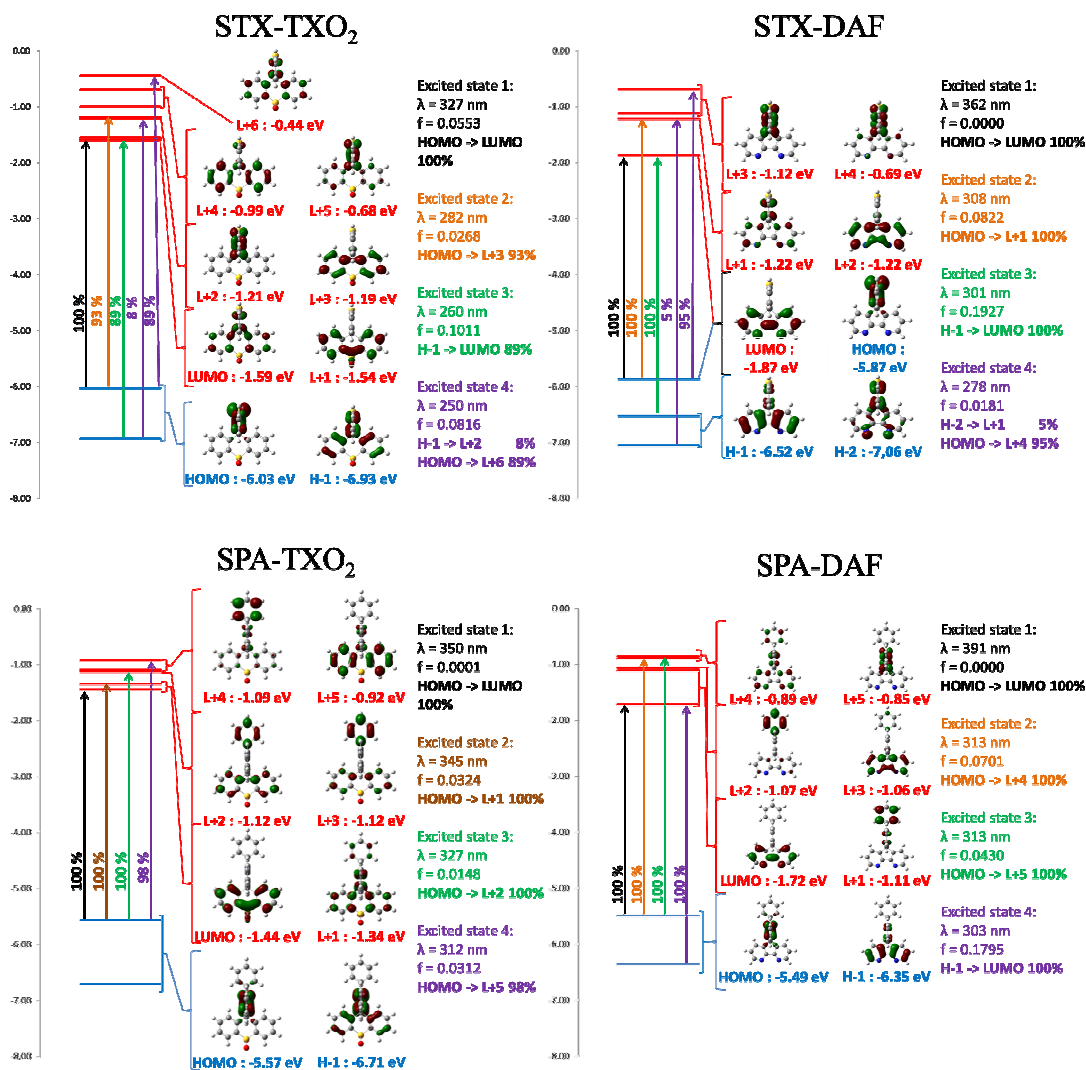


Figure 6. Calculated frontier molecular orbitals by DFT (B3LYP/6-311+G(d,p)) and the 4<sup>th</sup> first calculated electronic transitions by TD-DFT after geometry optimization with DFT B3LYP/6-311+G(d,p), shown with a isovalue of 0.04 [ $e \text{ bohr}^{-3}$ ]<sup>1/2</sup>

The calculated LUMO levels of **STX-DAF** and **SPA-DAF** are lower in energy (-1.87 and -1.72 eV resp.) than those of **STX-TXO<sub>2</sub>** and **SPA-TXO<sub>2</sub>** (-1.59 and -1.44 eV) clearly showing the stronger electron acceptor nature of the DAF unit compared to that of the TXO<sub>2</sub> unit. For the two DAF derivatives, the LUMO level is localized on the DAF fragment (in accordance with a first electrochemical reduction centred on this fragment, see above) and is separated by more than 0.6 eV from the LUMO+1 level. However, for the TXO<sub>2</sub> derivatives, the situation is slightly different. Indeed, the LUMO of **SPA-TXO<sub>2</sub>** is exclusively spread out on the TXO<sub>2</sub> core whereas that of **STX-TXO<sub>2</sub>** seems to be not only spread out on the TXO<sub>2</sub> core but also on the central TX unit. For both TXO<sub>2</sub> derivatives, the gap between the LUMO and the LUMO+1 is less than 0.1 eV (0.05/0.1 eV for **STX-TXO<sub>2</sub>** / **SPA-TXO<sub>2</sub>**) indicating some possible mixing of the LUMO and LUMO+1 orbitals. In conclusion the electronic separation between the donor (HOMO) and the acceptor unit (LUMO), key point in host

design, is clearly more efficient for the DAF derivatives than for the TXO<sub>2</sub> derivatives. The calculated energy gaps  $\Delta E_{\text{theo}}$ , follow the same trend than the electrochemical ones with the lowest gap calculated for **SPA-DAF** (3.77 eV) and the highest recorded for **STX-TXO<sub>2</sub>** (4.44 eV).

### Absorption spectroscopy

The UV-Visible absorption spectra of the four *D-spiro-A* dyes, recorded in cyclohexane, are presented in figure 7 and their main characteristics are summarized in table 2. The four compounds present different absorption spectra with three or four absorption bands with low absorption coefficients (between  $5 \times 10^3$  to  $20 \times 10^3$  L.mol<sup>-1</sup>.cm<sup>-1</sup>) in the range 260-350 nm. This is fully consistent with the presence of small and weakly conjugated units.

Absorption spectra of the two **TXO<sub>2</sub>** derivatives (Figure 7, left) are similar in the high energy range (maxima at 274/281 nm for **STX-TXO<sub>2</sub>** and at 273/280 nm for **SPA-TXO<sub>2</sub>**) indicating that these two absorption bands may be associated to the TXO<sub>2</sub> fragment. A series of previously reported TXO<sub>2</sub> derivatives spiro-linked to 2,7-triphenylamine-fluorene or to 2,7-N-phenylcarbazole fluorene also present absorption bands of the TXO<sub>2</sub> units close to 300 nm.<sup>51</sup>

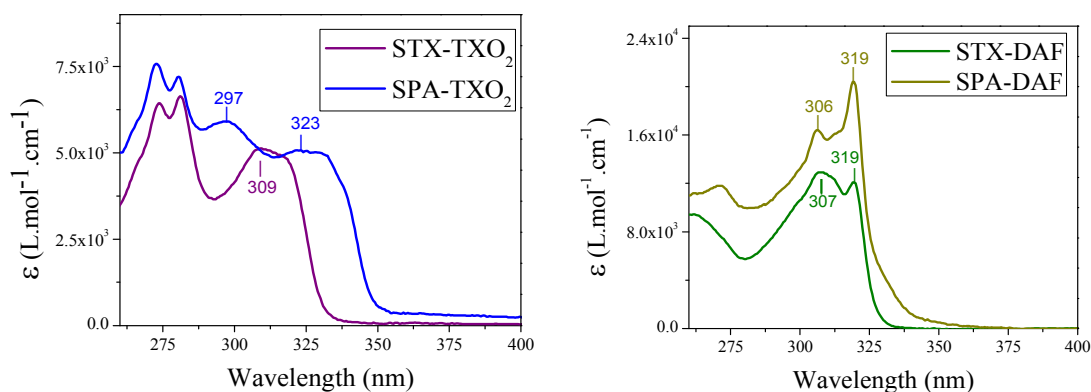


Figure 7. Absorption spectra of the four dyes in cyclohexane.

In the lowest energy range, the two spectra are nevertheless different with one broad band centred at 309 nm for **STX-TXO<sub>2</sub>** and two broad bands centred at 297 and 323 nm for **SPA-TXO<sub>2</sub>**. The band at 309 nm may therefore be associated to TX and the two bands 297 and 323 nm to PA. The absorption of TX has been previously reported and possesses a maximum centred at 266 nm in ethanol.<sup>74</sup> Thus, there is a red-shift of 43 nm between the absorption of TX and that of the spiro-bridged-TX recorded herein for **STX-TXO<sub>2</sub>**. A similar red shift of 32 nm has been reported for spiro-connected TX (bridged with a 2,7-triphenylamine-fluorene,  $\lambda^{\text{max}}$ : 298 nm in CH<sub>2</sub>Cl<sub>2</sub>).<sup>51</sup> This red shift is due to the different influence of a methylene bridge and of a spiroaromatic bridge on the TX core. Interestingly, absorption spectra of structurally related compounds built on the spiroconnection of PA units with anthracenone<sup>41</sup> present the same profile than that presented herein for **SPA-TXO<sub>2</sub>** with two absorption bands with maxima at 300/320 nm.<sup>41</sup>

The two DAF derivatives (Figure 7, right) present similar absorption spectra at lower energy, the absorption being however broader for **SPA-DAF** than for **STX-DAF**. The two main absorption bands centred at 306/307 and 319 nm may be assigned to the absorption of the DAF core in accordance with literature data.<sup>64, 66, 69, 75</sup> In addition, we have shown above that the band at 309 nm in **STX-TXO<sub>2</sub>** was assigned to the TX absorption. Thus, in **STX-DAF**, there is a clear superimposition of the absorptions of TX and DAF cores leading to a large band at 307 nm, being relatively more intense than that at 319 nm. Similarly, in the case of **SPA-DAF**, there is an overlap between the PA and DAF fragments, the shoulder observed above 327 nm being surely due to the absorption of the PA core. Finally, it should be stressed that higher absorption coefficients are obtained for **SPA-DAF** than for **STX-DAF** (**SPA-DAF**:  $\epsilon_{319\text{ nm}}=20.4\times 10^3\text{ L.mol}^{-1}.\text{cm}^{-1}$  and  $\epsilon_{306\text{ nm}}=16.4\times 10^3\text{ L.mol}^{-1}.\text{cm}^{-1}$ , **STX-DAF**:  $\epsilon_{319\text{ nm}}=12.1\times 10^3\text{ L.mol}^{-1}.\text{cm}^{-1}$  and  $\epsilon_{307\text{ nm}}=12.9\times 10^3\text{ L.mol}^{-1}.\text{cm}^{-1}$ ).

The calculated absorption spectra from TD-DFT (Figure 6) show that, except for **STX-TXO<sub>2</sub>**, the HOMO/LUMO transitions are theoretically forbidden (oscillator strength: 0.000). This is a crucial point, which finds its origin in the spatial separation of HOMO and LUMO levels leading to through space forbidden transitions. The calculated energy of this HOMO/LUMO transition varies from 327 nm for **STX-TXO<sub>2</sub>** to 391 nm for **SPA-DAF** when going from weak donor/acceptor units (TX and TXO<sub>2</sub>) to strong ones (PA and DAF). In **STX-TXO<sub>2</sub>**, as electronic densities of the HOMO and the LUMO allow some orbital overlap, the oscillator strength of the HOMO/LUMO transition is slightly higher (0.0553) and the transition is weakly allowed. Thus, in the case of DAF derivatives **SPA-DAF** and **STX-DAF**, the theoretical HOMO/LUMO transitions (391 and 362 nm *resp.*) are not detectable experimentally in their corresponding absorption spectra. Similarly, no band at 350 nm is observed for **SPA-TXO<sub>2</sub>**. Finally, the HOMO/LUMO theoretical transition calculated at 327 nm for **STX-TXO<sub>2</sub>** would be overlapped with the other absorptions bands.

Regarding the other transitions, one can note that a high oscillator strength ( $f>0.17$ ) transition is observed for both DAF derivatives. Indeed for both **STX-DAF** and **SPA-DAF**, HOMO-1/LUMO transitions between DAF units are detected at 301 nm and 303 nm *resp.* These oscillator strengths are in accordance with the high  $\epsilon$  recorded for these molecules (see above). For TXO<sub>2</sub> derivatives, the situation is different. Indeed, for **SPA-TXO<sub>2</sub>**, all the oscillator strengths are very low ( $f<0.033$ ), the more intense transitions being observed at 345 nm between HOMO and LUMO+1 ( $f = 0.0324$ ) and at 312 nm between HOMO and LUMO+5 ( $f=0.0312$ ). The transitions all involve PA units. In the case of **STX-TXO<sub>2</sub>**, all the oscillator strengths are also very low except a HOMO-1/LUMO transition ( $f= 0.1011$ ) with both orbitals involving TX and TXO<sub>2</sub> molecular fragments.

Optical gaps  $\Delta E_{\text{opt}}$  have been evaluated from the onset of the last absorption band, varying from 3.54 eV to 3.79 eV (**STX-TXO<sub>2</sub>** : 3.73 eV, **SPA-TXO<sub>2</sub>** : 3.54 eV, **STX-DAF** : 3.79 eV and **SPA-DAF** : 3.64 eV). Thus, one can note that **TXO<sub>2</sub>** derivatives present a  $\Delta E_{\text{opt}}$  in accordance with the electrochemical gap  $\Delta E_{\text{el}}$ , which is not the case for DAF derivatives (Table 1). Indeed, **STX-DAF** and **SPA-DAF** possess a  $\Delta E_{\text{opt}}$  strongly wider than their corresponding  $\Delta E_{\text{el}}$  (see Tables 1 and 2). Indeed and as exposed above, all molecules possess a theoretical forbidden through-space HOMO/LUMO transition, calculated at higher energy

for TXO<sub>2</sub> derivatives (327 and 350 nm) than for DAF derivatives (362 and 391 nm).  $\Delta E_{\text{opt}}$  should hence be determined with this absorption band. Thus, in the case of TXO<sub>2</sub> derivatives, this hypothetical transition would be overlapped in the tail of the large absorption band at 323 nm (**SPA-TXO<sub>2</sub>**) and 309 nm (**STX-TXO<sub>2</sub>**) whereas in the case of DAF derivatives this band would be found at lower energy (362 and 391 nm). Since  $\Delta E_{\text{opt}}$  does not correspond for DAF derivatives to the energy difference between HOMO and LUMO, this feature explains the difference observed between  $\Delta E_{\text{opt}}$  and  $\Delta E_{\text{el}}$ . As DAF derivatives present an almost identical  $\Delta E_{\text{opt}}$  (3.79 and 3.64 eV), the transition involved is surely a HOMO-1/LUMO transition implying for both compounds, only the DAF units (Figure 6).

### *Emission spectroscopy*

TX derivatives present structureless emission spectra with maxima recorded at 338 nm for **STX-TXO<sub>2</sub>** and at 348 nm for **STX-DAF** (Figure 8, left). Literature reports the emission of 4,5-diazaspirofluorene<sup>66</sup> at 350 nm (in THF) in accordance with that of **STX-DAF** and highlighting the weak influence of the spiroconnected unit (fluorene in diazaspirofluorene and thioxanthene in **STX-DAF**) on the DAF core. Emission of the PA derivatives also appear structureless and are red-shifted compared to those of TX derivatives ( $\lambda_{\text{max}}=348/350$  nm for **SPA-TXO<sub>2</sub>** /  $\lambda_{\text{max}}=388$  nm for **SPA-DAF**). Thus, one can observe a red shift of the emission maxima (and hence a gap contraction) as the donor and acceptor strength increases. It is important to mention that the emission of all compounds fits well with the energy of the HOMO/LUMO transition calculated by TD-DFT (**STX-TXO<sub>2</sub>**: 327 nm, **STX-DAF**: 350 nm, **SPA-TXO<sub>2</sub>**: 362 nm, **SPA-DAF**: 391 nm, see above). This clearly confirms the above mentioned assignment of a through space electronic transfer depending of the electrochemical HOMO/LUMO gap. The emission of the four dyes is hence due to a photoinduced intramolecular charge transfer (ICT) between the donor and the acceptor in the excited state (see below solvatochromic experiments). The more the donor-acceptor strength, the more contracted gap and the more red-shifted emission. Another signature of a through space electronic transfer is the very low quantum yield (QY) translating the very weak probability of this transition. In the present case, QY are indeed very low varying from 0.1 % for the two DAF derivatives to 0.8/4.1% for **SPA-TXO<sub>2</sub>**/**STX-TXO<sub>2</sub>** *resp.* in perfect accordance with our above mentioned conclusions. In addition, it should be noted that another emission of low intensity is detected at high energy (ca 330/350 nm) for **SPA-DAF**, which can be tentatively assigned to an emission induced by the fragments (PA or DAF) alone corresponding to a locally excited state or to an emission from a higher excited state. Indeed, for comparison purpose, the emission of triphenylamine is reported at 358 nm (in THF)<sup>76</sup> and that of N-phenyl-carbazole at 347 nm (in THF)<sup>76</sup> in accordance with the tiny band detected for **SPA-DAF**.



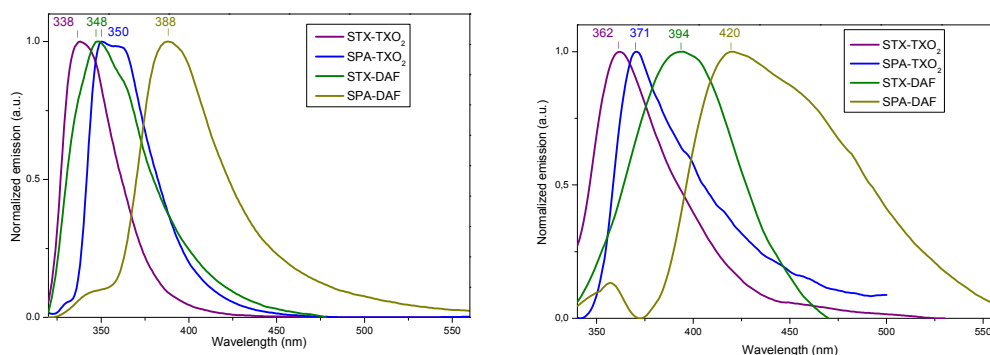


Figure 8. Emission spectra of the four dyes in cyclohexane (left) (concentration  $\sim 10^{-3}$  M) and in the solid state (thin film, deposited on a sapphire plate from 50  $\mu$ L of a 10 g/L solution) (right).

Regarding the solid state fluorescent properties (Figure 8-right), the emission spectra appear broader and red shifted (from 21 to 46 nm) compared to solution ones. This red shift is assigned not only to the different dielectric constants between the two environments (liquid vs solid) but also to the existence of intermolecular interactions in the solid state which may appear surprising due to the 3D geometry induced by the spiro carbon.

Table 2. Photophysical properties of the four dyes

	$\lambda_{\text{ABS}}$ (nm) [ $10^3 \cdot \epsilon$ (L.mol $^{-1}$ .cm $^{-1}$ )]	$\Delta E_{\text{OPT}}$ (eV) <sup>a</sup>	$\lambda_{\text{EM}}$ (nm) <sup>a</sup>	$\lambda_{\text{EM}}$ (nm) <sup>b</sup>	$\Delta\nu$ (cm $^{-1}$ / eV) <sup>a</sup>	$\Phi$ (%) [ $\lambda_{\text{exc}}$ (nm)] <sup>a</sup>	$E_{\text{T}}$ <sup>c</sup> (eV)	$\Delta S-T$ <sup>d</sup> (eV)
<b>STX-TXO<sub>2</sub></b>	309 (5.1); 281 (6.6); 274* (6.4)	3.73	338	362	2780 / 0.34	0.8 [308]	3.06	0.61
<b>SPA-TXO<sub>2</sub></b>	323(5.1); 297 (5.9); 280 (7.2); 273* (7.6)	3.54	350	371	2390 / 0.30	4.1 [323]	3.08	0.46
<b>STX-DAF</b>	319 (12.1); 307* (12.9)	3.79	348	394	2610 / 0.32	0.1 [319]	3.03	0.53
<b>SPA-DAF</b>	330(sh); 319(20.4); 306 (16.4); 271 (11.8)	3.64	388	420	5570 / 0.69	0.1 [319]	2.98	0.22

\*\  $\lambda_{\text{max}}$ , a\ in cyclohexane, b\ in thin film, c\ in frozen methylcyclohexane/2-methylpentane (1/1) (77 K), d\  $\Delta S-$

$$T = 1239.84 / \lambda_{\text{EM(cyclohexane)}} - E_{\text{T}}$$

Solvatochromic experiments allow going deeper in the understanding of the photophysical properties of the dyes through the determination of the polarity of the excited states (Table 3, Figure 9). First, as the absorption spectra do not differ much as a function of the polarity, the characteristics of the ground and Franck-Condon excited states are very similar (see SI). Oppositely, the fluorescence spectra show an intense solvatochromic effect. Indeed, the emission maxima of all fluorophores are red-shifted with the increase polarity of the solvent (from cyclohexane to acetonitrile, see Figure 9). This shift is of 58, 93, 110 and 111 nm for **STX-TXO<sub>2</sub>**, **STX-DAF**, **SPA-TXO<sub>2</sub>** and **SPA-DAF** respectively. The large bathochromic shift of the fluorescence emission is the consequence of the stabilization of intramolecular charge transfer (ICT) excited state relative to the ground state, leading to an energy gap contraction. This is caused by dipole-dipole interactions between the dyes and polar solvent molecules and hence of a photoinduced ICT between the donor and the acceptor.  $\Delta\mu$  of 13.4 D (**STX-TXO<sub>2</sub>**), 32.6 D (**SPA-TXO<sub>2</sub>**), 14.3 D (**STX-DAF**) and 29.2 D (**SPA-DAF**) have been evaluated using Lippert Mataga formalism (dipole moment at the ground state obtained through DFT calculations were: 4.8, 7.5, 3.1 and 6.2 D for **STX-TXO<sub>2</sub>**, **SPA-TXO<sub>2</sub>**, **STX-DAF** and **SPA-DAF** (see details for calculations in SI). We note that PA derivatives (**SPA-TXO<sub>2</sub>**,  $\Delta\mu$ : 32.6 D and **SPA-DAF**,  $\Delta\mu$ : 29.2 D) lead to a twice larger  $\Delta\mu$  than that calculated

for TX derivatives (**STX-TXO<sub>2</sub>**,  $\Delta\mu$ : 13.4 D and **STX-DAF**,  $\Delta\mu$ : 14.3 D). This reflects the stronger electron-donating ability of PA compared to TX and hence the stronger ICT induced.

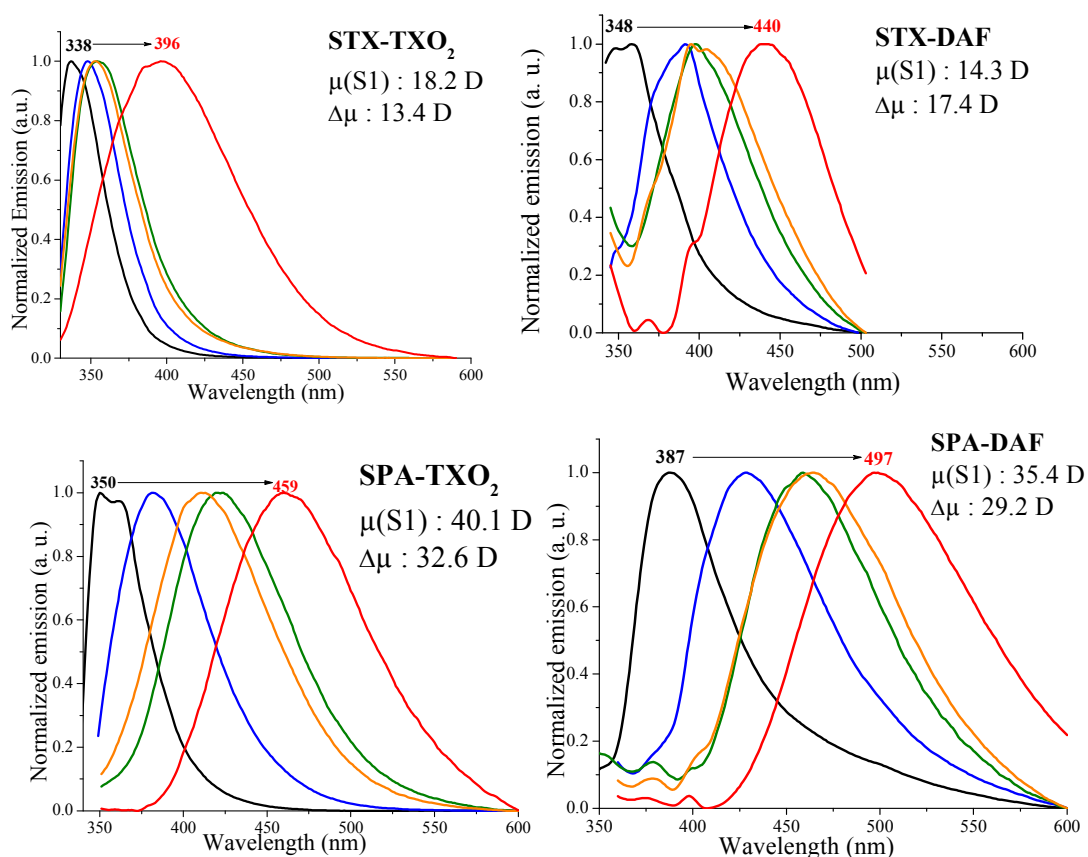


Figure 9. Normalized PL spectra of the four dyes in cyclohexane (black line); toluene (blue line), chloroform (green line), ethylacetate (orange line) and acetonitrile (red line).

Table 3. Photophysical properties of the four dyes as a function of the polarity of the solvents.

	$\lambda_{\text{abs}} \text{ (nm)} / \lambda_{\text{em}} \text{ (nm)} / \Phi \text{ (\%)} / [\lambda_{\text{exc}} \text{ (nm)}]$					$\Delta\mu / \mu(S1) / \mu(S0)^a$ (D)
	Cyclohexane	Toluene	Chloroform	Ethyl Acetate	Acetonitrile	
<b>STX-TXO<sub>2</sub></b>	309/338/0.8 [309]	311/348/0.7 [309]	312/354/0.7 [312]	310/353/0.9 [309]	310/396/1.1 [310]	13.4/18.2/4.8
<b>SPA-TXO<sub>2</sub></b>	324/350/4.1 [323]	326/382/2.3 [325]	328/421/1.2 [328]	326/410/1.7 [326]	300/460/1.4 [323]	32.6/ 40.1/7.5
<b>STX-DAF</b>	319/348/0.1 [319]	322/391/0.1 [321]	322/398/ 0.1 [322]	320/395/0.1 [319]	320/441/0.1 [319]	14.3/ 17.4/3.1
<b>SPA-DAF</b>	319/388/0.1 [319]	321/429/0.1 [321]	323/440/0.2 [332]	320/465/0.1 [319]	321/499/0.5 [320]	29.2/ 35.4/6.2

a.  $\mu(S0)$  has been obtained through DFT calculations,  $\Delta\mu$  has been obtained using Lippert-Mataga formalism,  $\Delta\mu = \mu(S1) - \mu(S0)$

Phosphorescence of the four dyes was studied at 77 K in frozen methylcyclohexane/2-methylpentane (1/1) (figure 10). TXO<sub>2</sub> derivatives present a first phosphorescent transition at 405/402 nm corresponding to an  $E_T$  of 3.06/3.08 eV for **STX-TXO<sub>2</sub>** and **SPA-TXO<sub>2</sub>**

respectively. For DAF derivatives, a first phosphorescence contribution is observed at 409 nm ( $E_T$ : 3.03 eV) for **STX-DAF** and at 416 nm ( $E_T$ : 2.98 eV) for **SPA-DAF**. In the light of these results, the spin density of the triplet state of the four molecules is probably located on their corresponding acceptor unit. This is a key point to be considered for the future design of structurally related host materials with a D-Spiro-A architecture. The four compounds present hence a very high  $E_T$  ( $3.03 \pm 0.05$  eV), enabling their use as host for blue dopant.

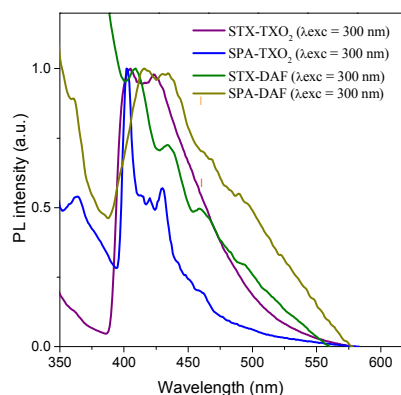


Figure 10. Emission spectra of the four dyes recorded at 77 K in frozen methylcyclohexane/2-methylpentane (1/1)

### Phosphorescent OLEDs.

Sky-blue (FIrpic) PhOLEDs were fabricated and characterised using the four host materials. The device configuration was ITO/CuPc (10 nm)/NPB (40 nm)/TCTA (10 nm)/EML: FIrpic (20 nm)/TPBi (40 nm)/LiF (1.2 nm)/Al (100 nm). ITO is used as the anode, CuPc (copper phthalocyanine) is the hole injecting layer, NPB (N,N'-di(1-naphthyl)-N,N'-diphenyl-[1,10-biphenyl]-4,4'-diamine) is the hole transporting layer, TCTA (4,4',4''-Tris(carbazol-9-yl)-triphenylamine) is the electron/exciton blocking layer, TPBi (1,3,5-Tris(1-phenyl-1H-benzimidazol-2-yl)benzene) is both the electron transporting layer and the hole blocking layer and a thin film of lithium fluoride covered with aluminium is the cathode. The device architecture and the relative energy levels of the successive layers can be found in our previous works.<sup>32,33</sup>

The four dyes were used as host for the sky-blue dopant FIrpic ( $E_T$ : 2.62 eV).<sup>\*77</sup> Different FIrpic concentrations were tested and the best performances were obtained with FIrpic 20 % doped EML. Those performances are reported in figure 11 and the main device characteristics summarized in table 4. The more efficient blue PhOLEDs were based on **SPA-DAF**, **STX-DAF** and **SPA-TXO<sub>2</sub>**, whereas devices using **STX-TXO<sub>2</sub>** as host were clearly less efficient.

\* The four dyes have been also used as host for green Ir(ppy)<sub>3</sub> and the devices performances are gathered in the SI.

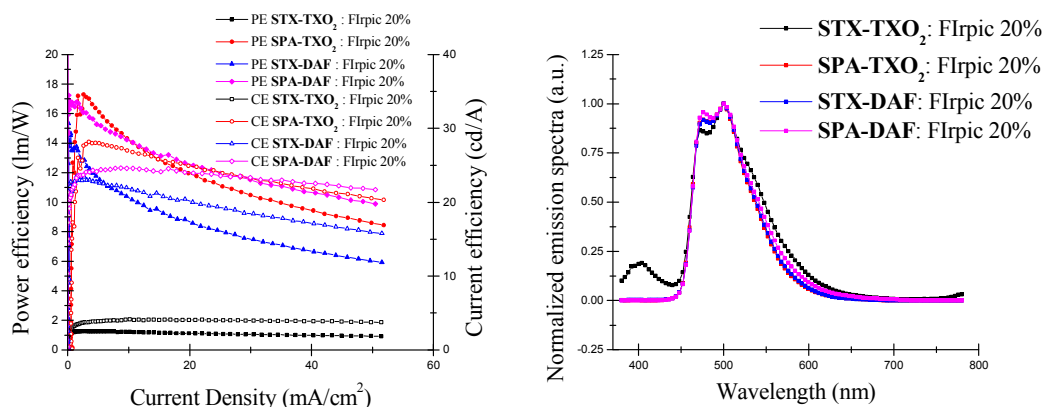


Figure 11. Current (empty symbol) and power efficiencies (filled symbol) versus current density of the blue devices using **STX-TXO<sub>2</sub>**, **SPA-TXO<sub>2</sub>**, **STX-DAF** and **SPA-DAF** doped with Flrpic 20 % in mass) as emitting layer (left). Corresponding EL spectra recorded at 10 mA/cm<sup>2</sup> (right).

In the TXO<sub>2</sub> family, PhOLEDs using **SPA-TXO<sub>2</sub>** as host reach a high EQE of 10.6 % (at 10 mA/cm<sup>2</sup>), whereas those using **STX-TXO<sub>2</sub>** as host are impressively less efficient displaying a very low EQE of 1.9 %. The corresponding luminous (CE) and power (PE) efficiencies are recorded at 27.7 cd/A and at 14.7 lm/W for **SPA-TXO<sub>2</sub>** and at 4 cd/A and at 1.2 lm/W for **STX-TXO<sub>2</sub>**. The devices incorporating DAF-derivatives do not display such difference as both display interesting performance at 10 mA/cm<sup>2</sup> with EQE of 8 % (CE= 22 cd/A and PE= 10.4 lm/W) and 10.2 % (CE= 24.3 cd/A and PE= 14 lm/W) for **STX-DAF** and **SPA-DAF** respectively.

Table 4. Selected EL data of blue devices

EML	V <sub>on</sub> (V)	CE (cd/A)		PE (lm/W)		EQE (%)	CIE (x;y)	L <sub>max</sub> (cd/m <sup>2</sup> ) (J <sup>b</sup> )
	L = 1 <sup>a</sup>	J = 1 <sup>b</sup>	J = 10 <sup>b</sup>	J = 1 <sup>b</sup>	J = 10 <sup>b</sup>	J = 10 <sup>b</sup>	J=10	
<b>STX-TXO<sub>2</sub> + 20%</b>	6.7	3.4	4.0	1.2	1.2	1.9	0.21; 0.41	1300 (70)
<b>SPA-TXO<sub>2</sub> + 20%</b>	3.1	17.1	27.7	12.3	14.7	10.6	0.17; 0.42	9200 (90)
<b>STX-DAF + 20%</b>	3.6	22.5	22.0	13.7	10.4	8.0	0.17; 0.42	4300 (60)
<b>SPA-DAF + 20%</b>	2.9	21.7	24.3	16.4	14.0	10.2	0.19; 0.43	6100 (70)

a) en cd/m<sup>2</sup>, b) en mA/cm<sup>2</sup>

From these blue PhOLED performances, several conclusions can be drawn. First, it is clear that the incorporation of PA units within the structure is strongly correlated to the high performance of the PhOLED. Thus, PhOLED performances based on the PA units are always higher than those based on the TX unit due to the higher HOMO energy levels measured for the former. In addition, **STX-TXO<sub>2</sub>** with the deepest HOMO and the highest LUMO levels in the series appears to be a very bad host material highlighting how an unsuitable combination can dramatically decrease the efficiency of a device. The potential of the DAF core is more difficult to evaluate. Indeed, the association of the DAF and TXO<sub>2</sub> fragments with the PA unit

leads to high performance devices with very similar efficiencies (Table 4, EQE of 10.6 % for **SPA-TXO<sub>2</sub>** and of 10.2 % for **SPA-DAF** at 10 mA/cm<sup>2</sup>). However, the association of the DAF and TX fragments in **STX-DAF** provides a PhOLED with an EQE four times higher than that of **STX-TXO<sub>2</sub>** (8% vs 1.9% *resp.*). The strong decrease of the LUMO level of **STX-DAF** compare to that of **STX-TXO<sub>2</sub>** leading to more efficient electron injection, may be involved in this impressive different efficiency. However, this effect is not found for **SPA-DAF** vs **SPA-TXO<sub>2</sub>** and more experiments would be therefore necessary to fully unravel this peculiar behaviour. We believe nevertheless that the potential of the TX unit is clearly not as high as that of the PA unit.

Except for **STX-TXO<sub>2</sub>** for which the performance is very low both in term of EQE (1.9 %) and in term of  $V_{on}$  (6.7 V), the *D-Spiro-A* design seems to be promising for hosting blue phosphors. Indeed, the present device performances are higher than those reported for non bipolar structurally related hosts such as the parent molecule **SBF** (EQE: 6.5 % at 10 mA/cm<sup>2</sup>).<sup>33</sup> As the device architecture of these previous works with **SBF** is the same as that presented herein (except the host material), the different performance can only be attributed to the nature of the host and more particularly to the adjustments of HOMO/LUMO energy levels. Similarly, 4-substituted **SBF** hosts, recently developed by our group such as 4-phenyl-**SBF** (EQE: 6 %),<sup>33</sup> 4-5-pyrimidinyl-**SBF** (5 %) <sup>78</sup> or 4-pyridinyl-**SBF**<sup>32</sup> (3.9 to 5.1%) all leads to lower blue PhOLED performance. Moreover, the present devices using **SPA-DAF**, **SPA-TXO<sub>2</sub>** and **STX-DAF** as host emit light at lower  $V_{on}$  (2.9 to 3.1 V for  $L=1$  cd/m<sup>2</sup>) than the above mentioned 4-phenyl-**SBF**,<sup>33</sup> 4-5-pyrimidinyl-**SBF**<sup>78</sup> and 4-pyridinyl-**SBF**<sup>32</sup> for which  $V_{on}$  are higher than 4 V. **SPA-DAF** and **SPA-TXO<sub>2</sub>** based blue PhOLEDs even surpass the performance of those based on the known and efficient host *N,N*-dicarbazolyl-3,5-benzene (*mCP*,  $E_T$ : 2.9 eV) previously reported in literature with exactly the same device architecture (EQE= 8.6 % at 10 mA/cm<sup>2</sup>,  $V_{on}$  = 3.2 V).<sup>45</sup> The better performance of the present hosts is due to their bipolar character, which allow a good adjustment of their HOMO/LUMO energy levels.

Interestingly, comparing the results obtained at 100 cd.m<sup>-2</sup> to those recorded at higher luminance (1000 cd.m<sup>-2</sup>), see SI, shows an increase of EQE for the three devices with **SPA-TXO<sub>2</sub>/STX-DAF** and **SPA-DAF** as host from 5.8/8.1 and 8.7 % to 10.8/8.3 and 10.2 % *resp.* These results show the stability and the efficiency of the devices even at high luminance.

All these features clearly highlight the efficiency of the *D-Spiro-A* design to host the sky blue phosphor *Flrpic*. Except the device using **STX-TXO<sub>2</sub>** as host, the EL spectra of the three other devices are identical (Figure 11 right), exclusively showing the emission of the blue dopant at 473 and 500 nm close to the photoluminescence of pure *Flrpic* film (475/500 nm) with no parasite emission.<sup>77</sup> The absence of other high energy emissions demonstrates an efficient energy transfer from the host to the guest. On the opposite, the EL spectrum of the device using **STX-TXO<sub>2</sub>** as host, presents in addition to the emission band of the dopant (*Flrpic*) another less intense emission centred at 400 nm in the range of the non-doped device emission (figure 11). This satellite emission and the lower efficiency of the device signs a less efficient energy transfer from **STX-TXO<sub>2</sub>** to *Flrpic*.

### Conclusion

The present work reports the synthesis, the physicochemical and photophysical properties and the application in sky blue PhOLED of four high triplet organic semi-conductors based on the *D-Spiro-A* design. This promising chemical design is based on a  $\pi$ -conjugation disruption induced by an insulating spiro bridge between a hole transporting unit, that is phenylacridine (PA) or thioxanthene (TX) moiety and an electron transporting unit that is dioxothioxanthene (TXO<sub>2</sub>) or diazafluorene (DAF) moiety. This molecular design leads to (i) a spatial separation of HOMO and LUMO retaining a high E<sub>T</sub>, (ii) HOMO/LUMO levels of the constituting building blocks adapted to efficient charge injections and (iii) good physical properties, key feature for device stability and performance. These host materials can be easily synthesized through a very short, efficient and highly adaptable synthetic strategy. In addition, we have shown that the properties of the dyes can be easily modulated depending of the strength of the donor/acceptor combination used, allowing to adjust the HOMO/LUMO levels without disturbing the E<sub>T</sub>. These molecules have been incorporated as host in sky blue PhOLEDs with EQE at 10 mA/cm<sup>2</sup> ranging from 2% to more than 10%. The best performance was obtained with **SPA-DAF** and **SPA-TXO<sub>2</sub>**, highlighting the importance of the chosen donor-acceptor combination on the device performance. We believe that the *D-Spiro-A* design is very promising to elaborate efficient host materials for blue PhOLED applications.

### ACKNOWLEDGMENT

We wish to thank the CDIFX (Rennes) for X-Ray diffraction data, the C.R.M.P.O for mass analysis, GENCI for allocation of computing time under project c2015085032 (Dr. F. Barrière, Rennes), the Institut des Sciences Analytiques (Villeurbanne) for TGA, the Service de Microanalyse-CNRS (Gif sur Yvette) for CHN analyses. MR, JRB and CP warmly thank the region Bretagne and the ADEME for a studentship (MR), Dr B. Laffite (ADEME), the CNRS and the ANR (Projects HOME-OLED n°11-BS07-020-01 and MEN IN BLUE n° 14-CE05-0024-01) for financial support.

### References

1. B. Geffroy, P. Le Roy and C. Prat, *Polym. Int.*, 2006, **55**, 572–582.
2. H. Sasabe and J. Kido, *Chem. Mater.*, 2011, **23**, 621-630.
3. Y.-S. Tyan, *J. Photon. Energy.*, 2011, **1**, 011009.
4. R. Mertens, *The OLED Handbook*, 2012, A guide to OLED Technology, Industry & Market, Ron Mertens, Edition 2012.
5. M. Romain, D. Tondelier, J.-C. Vanel, B. Geffroy, O. Jeannin, J. Rault-Berthelot, R. Métivier and C. Poriel, *Angew. Chem Int. Ed.*, 2013, **52**, 14147–14151.
6. N. Cocherel, C. Poriel, L. Vignau, J.-F. Bergamini and J. Rault-Berthelot, *Org. Lett.*, 2010, **12**, 452-455.
7. C. Poriel, N. Cocherel, J. Rault-Berthelot, L. Vignau and O. Jeannin, *Chem. Eur. J.*, 2011, **17**, 12631-12645.
8. D. Thirion, M. Romain, J. Rault-Berthelot and C. Poriel, *J. Mater. Chem.*, 2012, **22**, 7149-7157.
9. X. Yang, X. Xu and G. Zhou, *J. Mater. Chem. C*, 2015, **3**, 913-944.
10. H. Liang, X. Wang, X. Zhang, Z. Liu, Z. Ge, X. Ouyang and S. Wang, *New J. Chem.*, 2014, **38**, 4696-4701.
11. C. Liu, Q. Fu, Y. Zou, C. Yang, D. Ma and J. Qin, *Chem. Mater.*, 2014, **26**, 3074–3083.
12. L. Yao, S. Sun, S. Xue, S. Zhang, X. Wu, H. Zhang, Y. Pan, C. Gu, F. Li and Y. Ma, *J. Phys. Chem. C*, 2013, **117**, 14189-14196.
13. J.-H. Jou, S. Kumar, A. Agrawal, T.-H. Li and S. Sahoo, *J. Mater. Chem. C*, 2015, **3**, 2974-3002.
14. M. A. Baldo, D. F. O'Brien, M. E. Thompson and F. S. R., *Phys. Rev. B*, 1999, **60**, 14422.
15. M. A. Baldo, D. F. O'Brien, Y. You, A. Shoustikob, S. Sibley, M. E. Thompson and S. R. Forrest, *Nature* 1998, **395**, 151-154.
16. L. Xiao, Z. Chen, B. Qu, J. Luo, S. Kong, Q. Cong and J. Kido, *Adv. Mater.*, 2011, **23**, 926-952.
17. Y. Tao, C. Yang and J. Qin, *Chem. Soc. Rev.*, 2011, **40**, 2943-2970.
18. K. S. Yook and J. Y. L. Lee, *Adv. Mater.*, 2012, **24**, 3169-3190.
19. E. Mondal, W.-Y. Hung, Y.-H. Chen, M.-H. Cheng and K.-T. Wong, *Chem. Eur. J.*, 2013, **19**, 10563-10572.
20. C. Han, Z. Zhang, H. Xu, J. Li, G. Xie, R. Chen, Y. Zhao and W. Huang, *Angew. Chem. Int. Ed*, 2012, **51**, 10104-10108.
21. C. W. Lee and Y. J. Lee, *Chem. Mater.*, 2014, **26**, 1616-1621.
22. M. Romain, D. Tondelier, B. Geffroy, O. Jeannin, E. Jacques, J. Rault-Berthelot and C. Poriel, *Chem. Eur. J.*, 2015, **21**, 9426-9439.
23. C. Poriel, R. Métivier, J. Rault-Berthelot, D. Thirion, F. Barrière and O. Jeannin, *Chem. Commun.*, 2011, **47**, 11703-11705.
24. M. Romain, S. Thiery, A. Shirinskaya, C. Declairieux, D. Tondelier, B. Geffroy, O. Jeannin, J. Rault-Berthelot, R. Métivier and C. Poriel, *Angew. Chem Int. Ed.*, 2015, **54**, 1176-1180.
25. N. Fomina, S. E. Bradforth and T. E. Hogen-Esch, *Macromolecules*, 2009, **42**, 6440-6447.
26. S. Y. Hong, D. Y. Kim, C. Y. Kim and R. Hoffmann, *Macromolecules*, 2001, **34** 6474-6481.
27. S. Karabunarliev, M. Baumgarten, N. Tyutyulkov and K. Müllen, *J. Phys. Chem.*, 1994, **98** 11892-11901.
28. B. Pan, B. Wang, Y. Wang, P. Xu, L. Wang, J. Chen and D. Ma, *J. Mater. Chem. C*, 2014, **2**, 2466-2469
29. S. Gong, Y.-L. Chang, K. Wu, R. White, Z.-H. Lu, D. Song and C. Yang, *Chem. Mater.*, 2014, **26**, 1463-1470.
30. C. Fan, L. Zhu, T. Liu, B. Jiang, D. Ma, J. Qin and C. Yang, *Angew. Chem. Int. Ed*, 2014, **53**, 2147-2151.
31. M.-k. Leung, Y.-H. Hsieh, T.-Y. Kuo, P.-T. Chou, J.-H. Lee, T.-L. Chiu and H.-J. Chen, *Org. Lett.*, 2013, **15**, 4694-4697.
32. S. Thiery, D. Tondelier, C. Declairieux, B. Geffroy, O. Jeannin, R. Métivier, J. Rault-Berthelot and C. Poriel, *J. Phys. Chem. C*, 2015, **119**, 5790-5805.
33. S. Thiery, D. Tondelier, C. Declairieux, G. Seo, B. Geffroy, O. Jeannin, J. Rault-Berthelot, R. Métivier and C. Poriel, *J. Mater. Chem. C*, 2014, **2**, 4156-4166.

34. M.-k. Leung, W.-H. Yang, C.-N. Chuang, J.-H. Lee, C.-F. Lin, M.-K. Wei and Y.-H. Liu, *Org. Lett.*, 2012, **14**, 4986–4989.
35. C. Fan, Y. Chen, Z. Liu, Z. Jiang, C. Zhong, D. Ma, J. Qin and C. Yang, *J. Mater. Chem. C*, 2013, **1**, 463-469.
36. J. Zhao, G.-H. Xie, C.-R. Yin, L.-H. Xie, C.-M. Han, R.-F. Chen, H. Xu, M.-D. Yi, Z.-P. Deng, S.-F. Chen, Y. Zhao, S.-Y. Liu and W. Huang, *Chem. Mater.*, 2011, **23**, 5331-5339.
37. F. May, M. Al-Helwi, B. Baumeier, W. Kowalsky, E. Fuchs, C. Lennartz and D. Andrienko, *J. Am. Chem. Soc.*, 2012, **134**, 13818–13822.
38. J.-K. Bin, N.-S. Cho and J.-I. Hong, *Adv. Mater.*, 2012, **24**, 2911-2915.
39. J. Ding, Q. Wang, L. Zhao, D. Ma, L. Wang, X. Jing and F. Wang, *J. Mater. Chem.*, 2010, **20**, 8126-8133
40. H. Ohkuma, T. Nakagawa, K. Shizu, T. Yasuda and C. Adachi, *Chem. Lett.*, 2014, **43**, 1017-1019.
41. K. Nasu, T. Nakagawa, H. Nomura, C.-J. Lin, C.-H. Cheng, M.-R. Tseng, T. Yasuda and C. Adachi, *Chem. Commun.*, 2013, **49**, 10385-10387.
42. C.-J. Lin, H.-L. Huang, M.-R. Tseng and C.-H. Cheng, *J. Display Technol.*, 2009, **5**, 236-240.
43. Y.-X. Zhang, L. Zhang, L.-S. Cui, C.-h. Gao, H. Chen, Q. Li, Z.-Q. Jiang and L.-S. Liao, *Org. Lett.*, 2014, **16**, 3748–3751.
44. L. Ding, S.-C. Dong, Z.-Q. Jiang, H. Chen and L.-S. Liao, *Adv. Funct. Mater.*, 2015, **25**, 645-650.
45. M. Romain, D. Tondelier, B. Geffroy, A. Shirinskaya, O. Jeannin, J. Rault-Berthelot and C. Poriol, *Chem. Commun.*, 2015, **51**, 1313-1315.
46. B.-C. Wang, H.-R. Liao, J.-C. Chang, L. Chen and J.-T. Yeh, *J. Lumin.*, 2007, **127**, 333-342.
47. G. Méhes, H. Nomura, Q. Zhang, T. Nakagawa and C. Adachi, *Angew. Chem. Int. Ed.*, 2012, **51**, 11311-11315.
48. Z. Jiang, Z. Liu, C. Yang, C. Zhong, J. Qin, G. Yu and Y. Liu, *Adv. Funct. Mater.*, 2009, **19**, 3987-3995.
49. T. Liu, H. Sun, C. Fan, D. Ma, C. Zhong and C. Yang, *Org. Elec.*, 2014, **15**, 3568-3576.
50. H. Chen, Z.-Q. Jiang, C.-H. Gao, M.-F. Xu, S.-C. Dong, L.-S. Cui, S.-J. Ji and L.-S. Liao, *Chem. Eur. J.*, 2013, **19**, 11791-11797.
51. C.-Y. Chan, Y.-C. Wong, M.-Y. Chan, S.-H. Cheung, S.-K. So and V. W.-W. Yam, *Chem. Mater.*, 2014, **26**, 6585-6594.
52. Q. Zhang, J. Li, K. Shizu, S. Huang, S. Hirata, H. Miyazaki and C. Adachi, *J. Am. Chem. Soc.*, 2012, **134**, 14706–14709.
53. H. Li, A. S. Batsanov, K. C. Moss, H. L. Vaughan, F. B. Dias, K. T. r. Kamtekar, M. R. Bryce and A. P. Monkman, *Chem. Commun.*, 2010, **46**, 4812-4814.
54. Y. Li, Z. Wang, X. Li, G. Xie, D. Chen, Y.-F. Wang, C.-C. Lo, A. Lien, J. Peng, Y. Cao and S.-J. Su, *Chem. Mater.*, 2015, **27**, 1100-1009.
55. S.-J. Kim, J. Leroy, C. Zuniga, Y. Zhang, L. Zhu, J. S. Sears, S. Barlow, J.-L. Brédas, S. R. Marder and B. Kippelen, *Org. Electron.*, 2011, **12**, 1314-1318.
56. H. Sasabe, Y. Seino, M. Kimura and J. Kido, *J. Mater. Chem.*, 2012, **24**, 1404-1406.
57. F.-M. Hsu, C.-H. Chien, Y.-J. Hsieh, C.-H. Wu, C.-F. Shu, S.-W. Liu and C.-T. Chen, *J. Mater. Chem.*, 2009, **19**, 8002-8008.
58. S. O. Jeon, T. Earmme and S. A. Jenekhe, *J. Mater. Chem. C*, 2014, **2**.
59. K.-T. Wong, R.-T. Chen, F.-C. Fang, C.-c. Wu and Y.-T. Lin, *Org. Lett.*, 2005, **7**, 1979 - 1982.
60. W.-Y. Hung, T.-C. Wang, H.-C. Chiu, H.-F. Chen and K.-T. Wong, *Phys. Chem. Chem. Phys.*, 2010, **12**, 10685-10687.
61. H.-F. Chen, T.-C. Wang, W.-Y. Hung, H.-C. Chiu, C. Yun and K.-T. Wong, *J. Mater. Chem.* , 2012, **22**, 9658-9664.
62. C.-C. Chi, C.-L. Chiang, S.-W. Liu, H. Yueh, C.-T. Chen and C.-T. Chen, *J. Mater. Chem.*, 2009, **19**, 5561-5571.
63. W.-J. Li, B. Liu, Y. Qian, L.-H. Xie, J. Wang, S.-B. Li and W. Huang, *Polym. Chem.* , 2013, **4**, 1796-1802.



64. M. Hong, K. Zhang, Y.-Z. Li and J. Zhu, *Polyhedron*, 2009, **28**, 445-452.
65. X. Li, H.-J. Chi, G.-H. Lu, G.-Y. Xiao, Y. Dong, D.-Y. Zhang, Z.-Q. Zhang and Z.-Z. Hu, *Org. Elec.*, 2012, **13**, 3138-3144.
66. C.-C. Wang, C.-H. Yang, S.-M. Tseng, S.-Y. Lin, T.-Y. Wu, M.-R. Fuh, G.-H. Lee, K.-T. Wong, R.-T. Chen, Y.-M. Cheng and P.-T. Chou, *Inorg. Chem.*, 2004, **43**, 4781-4783.
67. H.-F. Chen, K.-T. Wong, Y.-H. Liu, Y. Wang, Y.-M. Cheng, M.-W. Chung, P.-T. Chou and H.-C. Su, *J. Mater. Chem.*, 2011, **21**, 768-774.
68. H.-F. Chen, W.-Y. Hung, S.-W. Chen, T.-C. Wang, S.-W. Lin, S.-H. Chou, C.-T. Liao, H.-C. Su, H.-A. Pan, P.-T. Chou, Y.-H. Liu and K.-T. Wong, *Inorg. Chem.*, 2012, **51**, 12114-12121.
69. C.-J. Zheng, J. Ye, M.-F. Lo, M.-K. Fing, X.-M. Ou, X.-H. Zhang and C.-S. Lee, *Chem. Mater.*, 2012, **24**, 643-650.
70. M. J. Plater, S. Kemp and E. Lattmann, *J. Chem. Soc., Perkin Trans. 1*, 2000, 971-979
71. G. R. Fulmer, A. J. M. Miller, N. H. Sherden, H. E. Gottlieb, A. Nudelman, B. M. Stoltz, J. E. Bercaw and K. I. Goldberg, *Organometallics*, 2010, **29**, 2176-2179.
72. T. P. I. Saragi, T. Spehr, A. Siebert, T. Fuhrmann-Lieker and J. Salbeck, *Chem. Rev.*, 2007, **107**, 1011-1065.
73. C. Poriel, J.-J. Liang, J. Rault-Berthelot, F. Barrière, N. Cocherel, A. M. Z. Slawin, D. Horhant, M. Virboul, G. Alcaraz, N. Audebrand, L. Vignau, N. Huby, G. Wantz and L. Hirsch, *Chem. Eur. J.*, 2007, **13**, 10055-10069.
74. R. Badiello, E. M. Fielden and S. C. Lillicrap, *Int. J. Radiat. Phys. Chem.*, 1973, **5**, 173-181.
75. R. P. Thummel, F. Lefoulon and R. Mahadevan, *J. Org. Chem.*, 1985, **50**, 3824-3828.
76. C.-C. Lee, M.-k. Leung, P.-Y. Lee, T.-L. Chiu, J.-H. Lee, C. Liu and P.-T. Chou, *Macromolecules*, 2012, **45**, 751-765.
77. E. Baranoff and B. F. E. Curchod, *Dalton Trans.*, 2015, **44**, 8318-8329.
78. S. Thiery, C. Declairieux, D. Tondelier, G. Seo, B. Geffroy, O. Jeannin, R. Métivier, J. Rault-Berthelot and C. Poriel, *Tetrahedron*, 2014, **70**, 6337-6351.

